PAPER • OPEN ACCESS

Coherent storage of temporally multimode light using a spin-wave atomic frequency comb memory

New Journal of Physics
The open access journal for physics

Coherent storage of temporally multimode light using a spin-wave atomic frequency comb memory

M Gündoğan[1], M Mazzera[1], P M Ledingham[1,3], M Cristiani[1] and H de Riedmatten[1,2]

[1] ICFO-Institut de Ciencies Fotoniques, Avenida Carl Friedrich Gauss 3, 08860 Castelldefels, Barcelona, Spain
[2] ICREA-Institució Catalana de Recerca i Estudis Avançats, 08015 Barcelona, Spain
E-mail: patrick.ledingham@icfo.es

New Journal of Physics **15** (2013) 045012 (16pp)
Received 11 January 2013
Published 19 April 2013
Online at http://www.njp.org/
doi:10.1088/1367-2630/15/4/045012

Abstract. We report on the coherent and multi-temporal mode storage of light using the full atomic frequency comb memory scheme. The scheme involves the transfer of optical atomic excitations in Pr^{3+} : Y_2SiO_5 to spin waves in hyperfine levels using strong single-frequency transfer pulses. Using this scheme, a total of five temporal modes are stored and recalled on-demand from the memory. The coherence of the storage and retrieval is characterized using a time-bin interference measurement resulting in visibilities higher than 80%, independent of the storage time. This coherent and multimode spin-wave memory is promising as a quantum memory for light.

[3] Author to whom any correspondence should be addressed.

Contents

1. Introduction

The coherent, efficient and reversible mapping between quantum light and matter represents a fundamental challenge in the field of quantum information science. Overcoming this challenge would enable the realization of a quantum memory for light, a device that can store and, on-demand, recall quantum states of light with high efficiency and fidelity. Such memories have potential applications for use in a quantum repeater [1–3], a resource allowing for quantum communication over long distances. Other applications include linear optics quantum computation [4], deterministic single-photon sources [5] and multi-photon quantum state engineering [6]. For practical applications, it is likely that a quantum memory with a high multimode capacity would be necessary.

One example of a quantum memory for light is a single atom trapped in a cavity [7]. An alternative candidate is the use of atomic ensembles [8]. The benefit of using such systems is that the light can be absorbed collectively, enhancing the coupling between light and matter. Indeed, extensive research effort has been put into single-atom and atomic ensemble-based memories alike. The realizations of ensemble-based memories include cold [9–14] and hot atomic gases [15–18] and solid state systems [19–37].

A promising ensemble-based quantum memory for light is the atomic frequency comb memory (AFC) [38] that is based on inhomogeneously broadened media, such as cryogenically cooled rare-earth ion-doped crystals. The AFC memory requires fine spectral tailoring of the inhomogeneously broadened absorption line into a series of equally spaced, narrow absorbing peaks. A resonant input pulse whose bandwidth matches that of the comb is collectively absorbed. This atomic coherence initially dephases, but due to the periodic structure of the comb, it rephases and coherently re-emits an echo. This light is in the same spatial mode as the input and at a delayed time of $\tau = 1/\Delta$, where Δ is the spectral distance between the peaks.

Recent progress on solid state quantum memories using the AFC scheme includes the storage of weak coherent pulses at the single-photon level [19, 22–24] and the storage of multiple temporal modes in a crystal [25, 26]. Storage of quantum light has also been demonstrated. The use of non-classical light generated by spontaneous parametric down conversion has enabled entanglement between one photon and one collective atomic excitation stored in a crystal [27, 28], entanglement between two crystals [29] and time-bin qubit storage [30]. Recently, the versatility of these memories was extended to the quantum storage of polarization qubits [31–33].

1.1. Three-level atomic frequency comb scheme

All of the above realizations used AFC storage in the excited state. However, strictly speaking, it is not an on-demand memory for light but rather a pre-programmed delay. In addition, the delay is limited to the excited state lifetime. On-demand retrieval of light, which is necessary for applications in quantum information science, can be achieved with a full AFC scheme which, as proposed in [38], transfers coherently the optical atomic excitation to and from a spin excitation. This proposal requires the use of three ground states. One is for the initial state (comb), one for the spin-wave excitations and a third one is needed as an auxiliary state for unnecessary ions that are not part of the AFC. The coherence needs to be transferred before the re-emission time τ. Once the coherence is transferred to a spin wave, for example by a single-frequency π-pulse, the dipole evolution is effectively frozen. To read out this spin wave, a second transfer pulse is applied after a time T_S, resulting in a three-level echo (3LE) with a total storage time of $\tau + T_S$. If each transfer pulse has an efficiency of η_T, then the total efficiency is given by [39]

$$\eta_{3LE} = \eta_{AFC}\,\eta_T^2, \tag{1}$$

where η_{AFC} is the two-level AFC echo efficiency. Assuming Gaussian absorbing peaks, the efficiency in the forward direction is approximated well by

$$\eta_{AFC} \approx \tilde{d}^2\, e^{-7/F^2}\, e^{-\tilde{d}}\, e^{-d_0}, \tag{2}$$

where $F = \Delta/\gamma$ is the finesse of the comb with γ being the peak width, $\tilde{d} = d/F$ is the effective optical depth experienced by the absorbed pulse with d being the optical depth and d_0 the absorbing background [38]. The transfer efficiency can be optimized by the use of chirped pulses as theoretically discussed in [40].

An additional benefit of the full AFC scheme is given by the presence of an extra degree of freedom related to the propagation direction of the control pulse. This allows for backward retrieval of the echo, enabling in theory a storage and retrieval efficiency of 100% [38]. Also, spatial separation of the control mode from the input mode is available.

A proof of principle of the full AFC scheme has been demonstrated using praseodymium-doped yttrium oxyorthosilicate ($Pr^{3+} : Y_2SiO_5$) with a total efficiency of 0.5–1% (transfer efficiency of 30–45%), with a multimode capacity of two temporal modes [39]. More recently, the full AFC scheme has been implemented in a different rare-earth ion sample ($Eu^{3+} : Y_2SiO_5$) [41] with a lower efficiency due to the low oscillator strength of the Eu^{3+} transition compared to Pr^{3+}. In this paper, using $Pr^{3+} : Y_2SiO_5$, we confirm for the first time the coherent nature of the storage explicitly by way of a time-bin interference measurement. Furthermore, we extend the efficiency and multimode capacity beyond what has been demonstrated previously. For this demonstration, we use bright pulses; however, the scheme is, in principle, extendable to the use of single photons as we will discuss later.

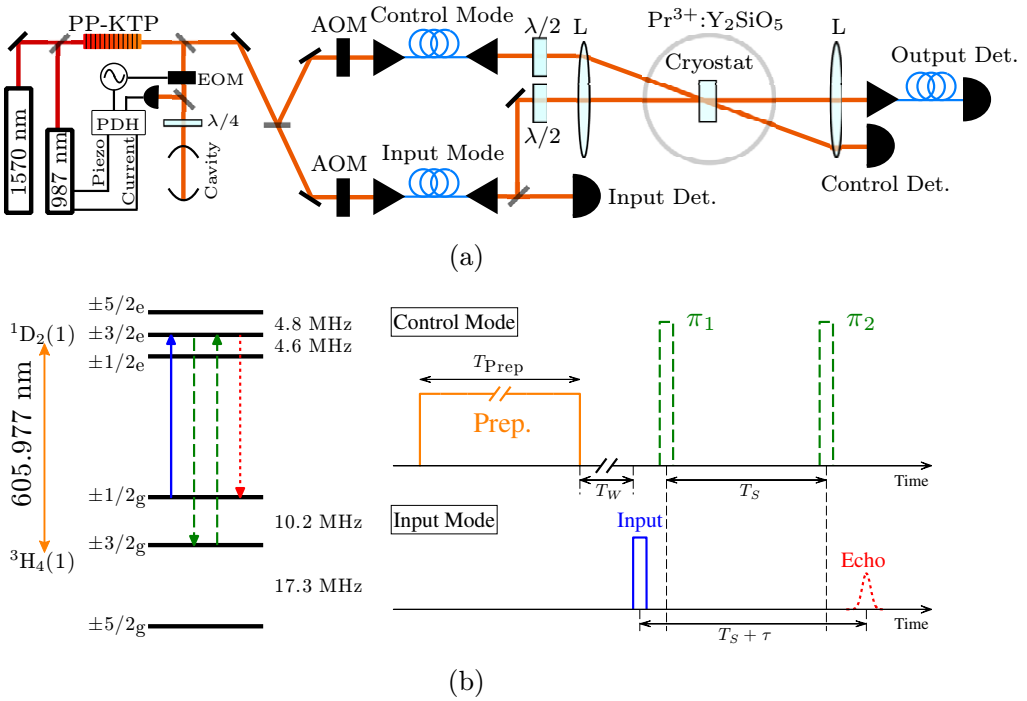

Figure 1. (a) Experimental setup. See the text for details. $\lambda/2$ ($\lambda/4$): half (quarter) wave plate; L: 100 mm lens; AOM: acousto-optic modulator in double-pass configuration; EOM: electro-optic modulator driven at 12.5 MHz; PDH: the Pound–Drever–Hall module for laser frequency locking. (b) Level scheme and pulse sequence for the spin-wave AFC memory. The comb is prepared in a time $T_{\mathrm{Prep}} = 200$ ms. A waiting time of $T_{\mathrm{W}} = 1$ ms is used between the end of the preparation and the start of the 3LE sequence. T_{s} is the time between the control pulses π_1 and π_2, and τ is the AFC delay time. The total storage time is $T_{\mathrm{S}} + \tau$.

1.2. Praseodymium

Cryogenically cooled $Pr^{3+} : Y_2SiO_5$ is an attractive medium for solid state quantum memories. Just as all the rare-earth ions, Pr^{3+} is characterized by a partially filled 4f shell spatially located within the full 5s and 5p ones. This feature allows Pr^{3+} to maintain an atomic-like energy level scheme, with homogeneous linewidth of the order of 2 kHz [42, 43], even when embedded in a crystalline matrix. Furthermore, the low nuclear magnetic moment of the neighbouring ions (Si and Y) prevents spin flips and magnetic ion–host interactions. A second-order hyperfine interaction is able to split the crystal field singlets into three sublevels, providing the threefold ground state required by the full AFC scheme. The optical transition used for the storage protocol connects the lowest-lying levels (labelled as (1)) of the ground $^3H_4$ and excited $^1D_2$ manifolds (see figure 1(b)), characterized by a wavelength of 605.977 nm. In samples doped with 0.02% Pr^{3+}, it has been reported to exhibit an inhomogeneous bandwidth of $\sim$5 GHz, which allows for tailoring the absorption profile into a frequency comb structure. The excited state has a lifetime of $T_1 = 164\,\mu$s and the coherence time with zero

magnetic field is $T_2 = 111\,\mu$s [42]. With the use of specific external magnetic fields [44] and dynamical decoupling sequences [45], light has been stored using electromagnetically induced transparency in $Pr^{3+} : Y_2SiO_5$ for times exceeding 1 s [46] and a hyperfine ground state coherence time exceeding 30 s has been demonstrated using similar techniques [47].

2. Experimental description

2.1. Optical setup

Figure 1(a) shows the experimental setup. Our laser source is based on sum frequency generation of 987 and 1570 nm light. These wavelengths are combined in a periodically poled potassium titanyl phosphate (PPKTP). With input power of 429 and 1138 mW and coupling efficiency into the waveguide of about 37.5 and 26.9% for the 987 and 1570 nm lasers, respectively, we achieve an output power of 190 mW at 606 nm, corresponding to a conversion efficiency of 385% W^{-1}.

Acousto-optic modulators (AOM) are used in double-pass configuration to create the necessary pulsed light for the echo experiments. This configuration allows to scan the frequency of the light by several MHz while keeping the intensity flat and spatial mode the same. The RF signals used to drive the AOMs are generated using an arbitrary waveform generator (Signadyne). We use two different optical paths to interact with the sample, the control and input modes, each having a double-pass AOM. The advantage of this choice is twofold. On the one hand, having a mode for the preparation and strong control light spatially separated from the input and weak echo light, prevents noise from the strong control mode polluting the echo mode. On the other hand, a strong control pulse might cause a free induction decay due to off-resonant excitation or an incorrectly prepared transparency window (see section 2.2). The echo would be hidden by this additional noise if the two modes were not spatially separated. These advantages become important from the perspective of single-photon level inputs.

After each AOM, the light is coupled to a single-mode fibre and then out-coupled on an isolated optical bench, where the closed cycle cryogenic cooler (Oxford V14) used for cooling the crystal to 2.8 K is located. Our $Pr^{3+} : Y_2SiO_5$ sample is 3 mm thick with 0.05% doping. The absorption coefficient is measured to be $\alpha = 23\,\text{cm}^{-1}$ for the optical transition at 605.977 nm. The inhomogeneous linewidth is measured to be 5 GHz. Half-wave plates ($\lambda/2$) ensure that the polarization is aligned parallel to the optical D_2-axis of the crystal, in order to maximize the absorption [43]. A glass plate is placed in the input mode allowing a reference signal on the input detector. An $f = 100$ mm lens is used to focus both modes on to the crystal, resulting in a beam width size of around 95 μm for both the control and input modes. The maximum power in the control mode before the cryostat window is measured to be 7 mW. The maximum power available in the input mode is 1.5 mW. An additional $f = 100$ mm lens is placed after the crystal for spatial mode matching. The echo mode is steered to a detector via a single-mode fibre with 50% coupling efficiency.

The 606 nm light is frequency locked to a passively stabilized cavity using the Pound–Drever–Hall locking technique [48]. This method of locking provides the desirable laser linewidth for the fine spectral tailoring of the AFC, as well as long-term frequency stability. The setup schematic is shown in figure 1(a). The cavity has a free spectral range of 1 GHz and a linewidth of 1.45 MHz leading to a finesse of 690. A temperature stabilized Invar spacer is used to hold the cavity mirrors. Light used for locking is picked off before the AOMs and

directed through an electro-optic modulator (EOM). The EOM is driven by an RF source (Toptica Digilock module) resulting in phase-modulated sidebands at 12.5 MHz. The error signal is created using in-house electronics and is fed-back to the piezo and current drivers of the 987 nm laser via the Toptica Digilock and fast analogue linewidth control (FALC 110) modules, respectively. Spectral hole-burning experiments reveal the laser linewidth to be around 100 kHz for ms timescales.

2.2. Memory preparation

The scheme of the full AFC protocol realized in this work is depicted in figure 1(b). The input pulse (solid arrow) is resonant with the comb on the $1/2_g$–$3/2_e$ transition, while the coherent transfer of the optical excitation to and from the ground state (dashed arrows) is tuned to the $3/2_g$–$3/2_e$ transition. The echo is emitted on the $1/2_g$–$3/2_e$ transition (dotted arrow). The remaining $5/2_g$ ground level is exploited as the auxiliary state.

The preparation of the memory follows the approach described in [49]. A transparency window is first created inside the absorption profile with the procedure hereby described. The laser frequency is swept by 12 MHz using an AOM, thus pumping all the ions that are resonant with this light to a non-resonant ground state. The sweep is repeated 100 times, resulting in a transparency window (the 'pit') with a width (full-width at half-maximum) of 18 MHz [49, 50]. To tailor the AFC, the burn-back method is used. It consists of the pumping of ions from the $5/2_g$ auxiliary state, some of which will decay in the ground states previously emptied, giving rise to isolated narrow peaks in the transparency window. By sending several burn-back pulses at frequencies differing by Δ, the AFC structure is created. The finesse of the comb, and thus the efficiency of the AFC echo, can be optimized with a proper choice of duration, power and the number of the burn-back pulses.

It is important to note that, since the hyperfine level splittings ($\sim$ MHz) are smaller than the inhomogeneous width ($\sim$ GHz), different classes of ions will be resonant with the burn-back pulses [50]. In the frequency window of interest for the comb, transitions associated with two classes of ions are indeed present (namely, $1/2_g$–$3/2_e$ of class I and $1/2_g$–$1/2_e$ of class II).

The burn-back procedure also populates the $3/2_g$ ground state, while an efficient full AFC scheme requires it to be empty. As a matter of fact, if some ions remained in the ground state addressed by the control pulse, they would be driven to the excited state and give noise in the echo mode due to spontaneous emission. To avoid this additional noise, a further 'clean' sweep is performed in the spectral region of the $3/2_g$–$3/2_e$ transition whose bandwidth matches that of the comb. This clean sweep offers also the ulterior advantage of emptying the ground states of the unwanted classes.

In this paper, the total preparation time, T_{Prep} from figure 1(b), is 200 ms, of which 50 ms are used to create the comb. This includes $5 \times 100\,\mu$s burn-back pulses for the five comb peaks repeated every 500 ns for 100 times and a 2 MHz clean sweep centred at the transfer pulse frequency repeated 1000 times.

For the experimental results presented in the next section, we use different detection methods. For the results presented in sections 3.1–3.4 a photodiode (Thorlabs PDB150) is used and a memory is prepared for each pulse that is stored. For section 3.5 a single-photon counter (Laser Components, model Count) is used and for each memory prepared, 500 pulse trains are used.

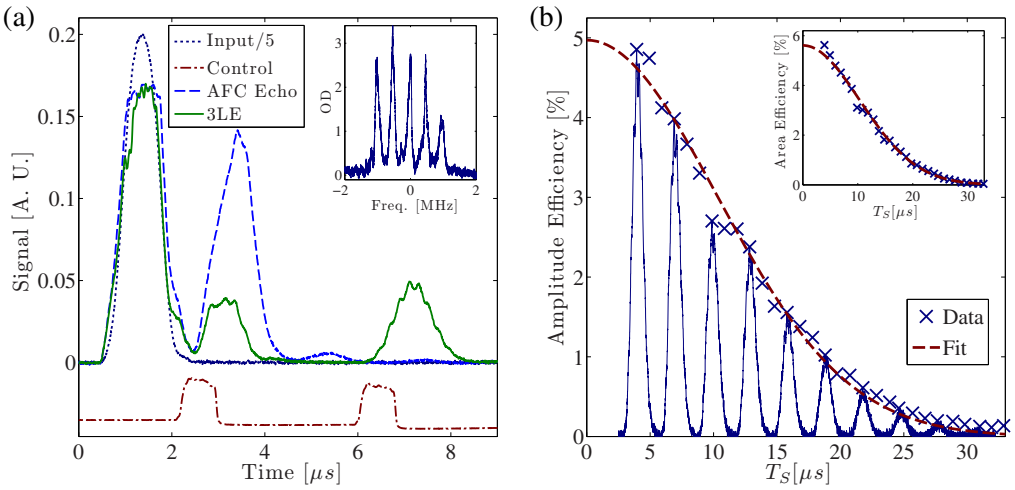

Figure 2. (a) The full AFC memory scheme. The blue dashed curve shows the two-level echo from an AFC programmed to give a delay of 2 μs ($\Delta = 500$ kHz). The green solid curve shows the effect of the transfer pulses. The AFC echo is reduced and the 3LE is observed. The dark blue dotted trace shows a reference of the input pulse, with a full-width at half-maximum duration of 840 ns. For clarity, this curve is divided by 5. The dot-dashed trace indicates the temporal location of the 800 ns rephasing pulses separated by $T_S = 4\,\mu$s. The inset shows a single-shot measurement of a comb with $\Delta = 500$ kHz. (b) 3LE efficiency versus T_S for the same conditions as in (a). All curves and data points are the average of ten experimental runs.

3. Results

3.1. Atomic frequency comb storage

Figure 2(a) shows an example of a two-level AFC echo (dashed curve) for an excited state storage time of $\tau = 2\,\mu$s. In the inset an example of comb with a periodicity $\Delta = 500$ kHz is represented for illustrative purposes. It is worth noting that the read method and the limited detection response time lead to underestimation of the comb optical density and finesse. Using input pulses of 840 ns duration, an AFC efficiency of $\eta_{\mathrm{AFC}} = 15.6 \pm 0.5\%$ is observed. The efficiency is measured by taking the area of the echo in the blue dashed trace and comparing this with the area of the input pulse when sent through a spectral pit (dark blue dotted trace). When measuring the input pulse area, its polarization is rotated to be perpendicular to the optical D_2-axis, ensuring weak interaction with any residual ions in the pit. To estimate the parameters of the comb, we compare the area of the transmitted pulse to that of the echo [19]. Assuming a tooth width of $\gamma = 125\,(167)$ kHz, then $F = 4\,(3)$ and the inferred optical depths are $d = 4.12\,(3.66)$ and $d_0 = 0.45\,(0.26)$.

3.2. Spin-wave storage

Figure 2(a) shows an example of the full AFC scheme of spin-wave storage (solid curve). A strong single-frequency control pulse is used to transfer the excited state coherence to and from the $3/2_g$ ground state. The effect of the first transfer pulse is clearly seen from the

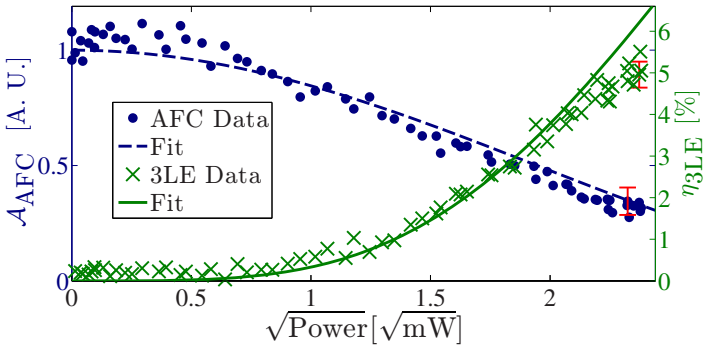

Figure 3. Two-level AFC echo area $\mathcal{A}_{\mathrm{AFC}}$ (dots) and three-level efficiency $\eta_{3\mathrm{LE}}$ (crosses) as a function of the square root of power of the control pulses. The dashed and solid lines represent a fit to the data as described in the text. Each data point is the average of ten trials. Error bars indicate the maximum standard error in the mean measured for each data set.

significant reduction of the AFC echo. A second transfer pulse is applied after a time $T_{\mathrm{S}} = 4\,\mu\mathrm{s}$ and a 3LE is clearly seen above the noise. It is a direct result of the application of both control pulses, as confirmed by the fact that it vanishes on removing either π_1, π_2 or the input itself.

Figure 2(b) shows the 3LE efficiency, both amplitude and area (inset), as a function of T_{S}. Due to the inhomogeneous broadening of the spin state, the efficiency of the echo decays as a function of T_{S}. This inhomogeneity is known to be Gaussian with the following form [41]:

$$\eta(T_{\mathrm{S}})_{3\mathrm{LE}} = \eta(0)_{3\mathrm{LE}} \times \exp\left[\frac{-(\gamma_{\mathrm{IS}} T_{\mathrm{S}})^2}{2\log(2)/\pi^2}\right], \tag{3}$$

where γ_{IS} is the spin inhomogeneous broadening and $\eta(0)_{3\mathrm{LE}}$ is the 3LE efficiency at zero delay. Fitting the data with this equation and extrapolating to $T_{\mathrm{S}} = 0$ where the spin inhomogeneity has no effect, the 3LE efficiency ($\eta(0)_{3\mathrm{LE}}$) for the area (amplitude) is $5.6 \pm 0.1\%$ ($5.0 \pm 0.1\%$). The corresponding inhomogeneity is $\gamma_{\mathrm{IS}} = 25.6 \pm 0.2\,\mathrm{kHz}$ ($25.7 \pm 0.4\,\mathrm{kHz}$), in agreement with previous realizations [39, 51]. Comparing the AFC efficiency with this 3LE efficiency, the transfer efficiency is calculated to be 57–60% using equation (1).

An alternative method for assessing the transfer efficiency is to compare the area of the AFC echo to that reduced by the first control pulse. From figure 2(a), we get $\eta_{\mathrm{T}} = 73\%$ for $T_{\mathrm{S}} = 4\,\mu\mathrm{s}$. This is higher than what is obtained from the 3LE. The disagreement could be due to the imperfect spatial mode overlap between the control and input modes.

This is the full AFC scheme with the highest efficiency reported so far. Nevertheless, in view of applications in quantum communication, further improvements are necessary as we will discuss later.

3.3. Transfer characterization

We now characterize the transfer efficiency η_{T} as a function of the power in the control pulse and thus the Rabi frequency (Ω_{R}). The experimental conditions for this measurement are identical to those outlined in figure 2(a). A time T_{S} of $4\,\mu\mathrm{s}$ is chosen as a time fast compared to the spin inhomogeneous dephasing time so as not to limit the efficiency.

Figure 3 shows the 3LE efficiency and the area of the AFC echo $\mathcal{A}_{\mathrm{AFC}}$ as a function of the square root of power of the control pulse. Intuitively, as the power is increased the AFC

echo decreases and the 3LE increases. This behaviour can be modelled simply with a two-level atomic system being driven resonantly [52, 53], resulting in the following equations:

$$\mathcal{A}_{\mathrm{AFC}}(\bar{\Omega}_{\mathrm{R}}t) = \mathcal{A}_{\mathrm{IN}}\frac{\eta_{\mathrm{AFC}}}{2}\left[1+\cos(\bar{\Omega}_{\mathrm{R}}t)\right], \tag{4}$$

$$\eta_{\mathrm{3LE}}(\bar{\Omega}_{\mathrm{R}}t) = \frac{\eta_{\mathrm{AFC}}}{4}\left[1-\cos(\bar{\Omega}_{\mathrm{R}}t)\right]^2, \tag{5}$$

where $\mathcal{A}_{\mathrm{IN}}$ is the area of the input pulse and we introduce $\bar{\Omega}_{\mathrm{R}}$ as the effective Rabi frequency. This takes into account that the input and control pulses have inhomogeneous spectral and spatial profiles and also the imperfect spatial mode overlap between the two modes. The data in figure 3 are fit simultaneously with the above equations and show good agreement. The effective Rabi frequency is found to be $\bar{\Omega}_{\mathrm{R}} = 2\pi \times 340\,\mathrm{kHz}$ for a power of 5.7 mW at the crystal.

For a comparison, we measure the Rabi frequency with coherent hole burning techniques [54] using only the control mode, resulting in $2\pi \times 420\,\mathrm{kHz}$. Finally, knowing the oscillator strength of the transition [49, 50] and the laser intensity, we calculate the expected Rabi frequency to be about $2\pi \times 430\,\mathrm{kHz}$. This Rabi frequency is independent of spectral inhomogeneity and spatial mode overlap, and is therefore higher than the effective Rabi frequency.

3.4. Coherent storage

In order to implement a quantum memory, it is crucial that the phase between two modes is preserved during storage and retrieval. For quantum communication schemes, information is often encoded into the amplitude and phase of time-bin qubits, as they are known to be robust against decoherence in optical fibres [55]. We confirm for the first time the coherent storage of time-bin information using the spin-wave AFC memory.

To verify the coherence of the storage, we send a pair of pulses (I_e and I_l) separated by t_{s} and with a relative phase difference ϕ. The pair of pulses is stored and analysed directly in the memory. This requires the implementation of partial readouts [56], achieved by sending two readout pulses (π_2 and π_3) separated also by t_{s} (see the upper panel of figure 4(a)). The resulting output of the memory is three temporal modes, where the central mode shows coherent interference between the echo of the late pulse from the first readout and the echo of the early pulse induced by the second readout ($E_{l1} + E_{e2}$).

Figure 4(b) shows an interference fringe of the central output mode as the relative phase difference ϕ is changed for $\tau = 5\,\mu\mathrm{s}$, $T_{\mathrm{S}} = 12\,\mu\mathrm{s}$, $\mathrm{t_s} = 1\,\mu\mathrm{s}$ and pulse durations of 700 ns. For each phase, a total of ten trials is made for statistics. The detection window width $\mathrm{t_v}$ is chosen to be 500 ns. The data clearly show coherent behaviour with a weighted sinusoidal fit giving a visibility of $84.0 \pm 5.7\%$.

The coherent nature of the storage is probed further by investigating the fringe visibility as a function of T_{S}. Shown in the lower panel of figure 4(a), the visibility remains at a constant value of $\bar{V} = 81.7 \pm 1.4\%$ as T_{S} is increased, i.e. is independent of the storage efficiency. This behaviour is typical of ensemble-based quantum memories [57], where atomic decoherence decreases the efficiency of recall but not the conditional fidelity. This is true as long as the signal is much greater than the background noise, which may prove challenging to achieve for single photon level inputs. For a comparison, we repeated the experiment while changing the relative phase of the readout pulses, and also obtained an interference fringe with $V = 84\%$.

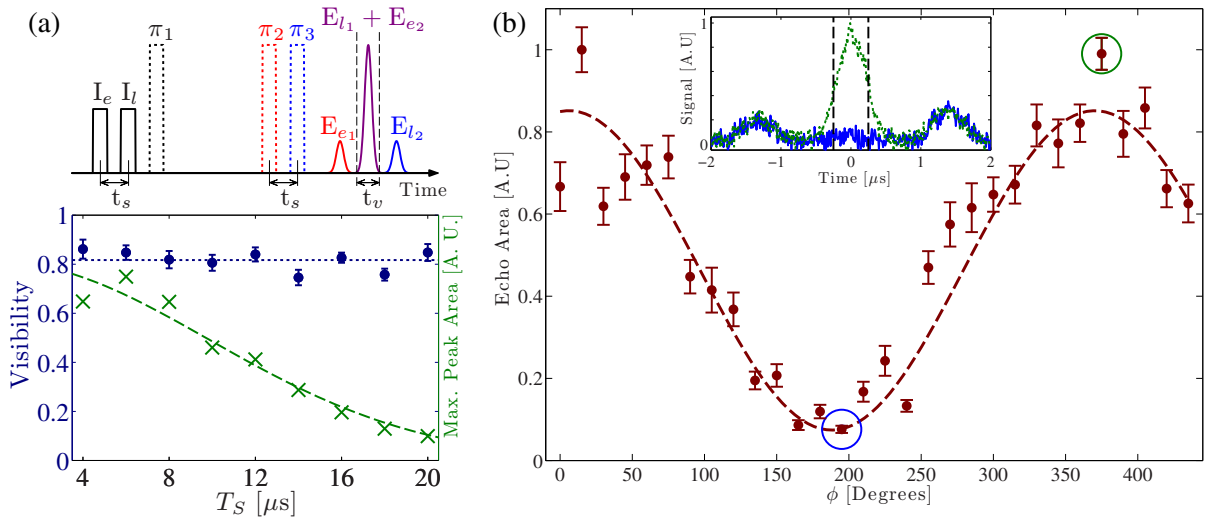

Figure 4. (a) Upper panel: the pulse sequence used for the interference experiment. Lower panel: visibility and maximum peak area versus T_S. The dots (crosses) correspond to the measured visibility (area). For each T_S, a curve like (b) is measured from which the visibility is extracted via a weighted fit. The error bar is a confidence interval of this fit of one standard deviation. The horizontal dotted line is the mean of the visibilites, $\bar{V} = 81.7 \pm 1.4\%$. The dashed line is a fit using equation (3) with a corresponding spin inhomogeneity of $\gamma_{IS} = 26.8 \pm 1.7$ kHz. (b) Echo area in the interference window versus phase difference between the two input pulses. Each data point is the average over ten trials with the error bar representing one standard deviation of the mean. The dashed line is a weighted fit of the data to a sine. The visibility is $84.0 \pm 5.7\%$. Inset: time-bin qubit interference for a phase difference of 195° (solid line) and 375° (dotted line). The corresponding data points in the main figure are labelled with circles. The vertical dashed lines indicate the interference window ($t_v = 500$ ns).

The observed visibilities would result in storage conditional fidelities exceeding 90% ($F_C = (1 + V)/2$), which, if this could be demonstrated with single photon fields, would be sufficient for application in quantum communication. The maximal possible visibility should however be 100%. Note that, besides the possible decoherence in the crystal, the visibility is directly affected by the phase noise between the two input time bins and between the two control pulses. To test this phase noise, we carried out an interference measurement using two pulse photon echoes (i.e. without transfer to the ground state). The resulting visibilities were similar, confirming that storing in the ground state does not affect the coherence. Also, this indicates that the main source of decoherence is the limited coherence of the laser itself and not the storage and retrieval process.

3.5. Multimode storage

An important feature of a quantum memory is its multimode capacity. A memory exhibiting this property allows for multiplexing, which, for example, can increase the success rate of a

quantum repeater by a factor given by the multimode capacity [58]. Temporal multimodality has been demonstrated with the two-level AFC [25, 26], but most implementations have used systems that do not have three ground states and are thus not extendible to the full scheme.

As stated in [39], the maximum multimode storage capacity (N_{max}) is limited by the number of teeth (N_{teeth}) in the comb. This can be understood in terms of the ratio between the duration of each input mode and the total duration of the pulse train. The former is limited by the comb bandwidth. The latter is limited by the AFC storage time and thus by the width and the number of teeth that can fit in the comb bandwidth.

For the two-level AFC experiments, a great deal of effort has been made to increase the comb width [25], up to GHz bandwidth [26, 28]. However, this is not possible for three-level AFC experiments, since the comb bandwidth is determined by the hyperfine splitting, which ranges from a few MHz for Pr-doped solids to tens of MHz for Eu-doped solids. In order to increase the multimode capacity for spin-wave storage, the difficulty is then to reduce as much as possible the AFC peak widths, which requires a narrow line preparation laser. For our system, the limiting hyperfine splitting is the excited state one ($\sim$5 MHz), while our tooth width is fixed by the laser linewidth of $\sim$100 kHz. The ultimate limit on the tooth width is given by the homogeneous width of the praseodymium ion ($\sim$2 kHz) [42].

Another parameter affecting the storage efficiency that should be taken into account is the temporal duration of the control pulses. In the ideal case, their bandwidth matches that of the comb. In fact, the duration of the π-pulse, and thus the bandwidth of the memory, is determined by the available Ω_{R}. For a limited Ω_{R}, efficient transfer between optical and spin-wave atomic excitations requires long control pulses, which in turn requires long input pulses. This limits the number of modes that can be stored. With this in mind, extension to an efficient multimode spin-wave memory is non-trivial.

The application of several strong input modes to a single-class comb can either induce the emission of a two-pulse photon echo, accumulated echo, or in the worst case, destroy the comb itself. To avoid the occurrence of these undermining events, the storage of multiple modes is carried out with low-power input pulses ($\sim 2 \times 10^4$ photons per pulse) and the recalled echoes are detected with a single-photon detector (SPD; model Count, Laser Components). Neutral density filters (OD = 6.5) are placed after the crystal to avoid saturating the detector. Moreover, a double-pass AOM is used to temporally gate any noise from the control mode polluting the output mode. For each memory prepared, a total of 500 pulse trains are sent. The electronic signal from the SPD is sent to a time-stamping card which collects the arrival times in a histogram.

Figure 5 shows an example of five temporal modes stored and retrieved using the full AFC scheme. An AFC storage time $\tau = 7\,\mu$s (corresponding to comb teeth separated by $\Delta = 133$ kHz) was programmed, with a bandwidth of 2 MHz ($N_{\mathrm{teeth}} = 15$). A total of 1×10^5 (2×10^6) pulse trains were used to observe the AFC (3LE) echo. The requirements of a long AFC storage time and of short input pulses contribute to the decrease of the 3LE efficiency with respect to the optimized case of a single mode shown in figure 2(a). Indeed, both the two-level AFC echo and the transfer efficiency are decreased compared to figure 2(a). In fact, the total efficiency for the storage and retrieval of five modes is here limited to 0.1%. A confirmation of the fact that the overall efficiency strongly depends on the AFC storage time comes from the inset of figure 5, which shows the 3LE efficiency as a function of the temporal mode number. As the number of modes is decreased, a shorter AFC storage time is used and

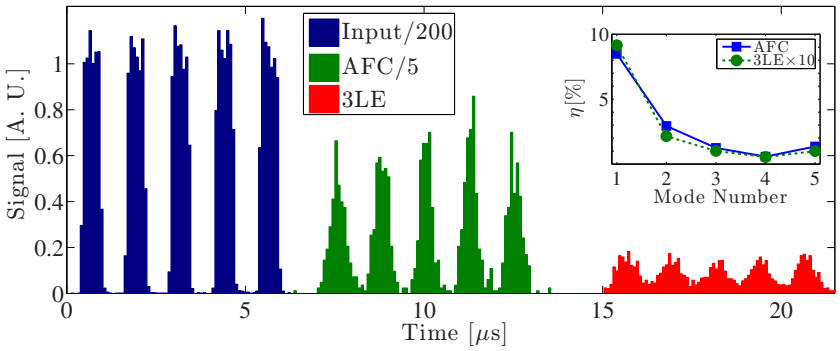

Figure 5. Three-level storage of five temporal modes. The AFC delay is $\tau = 7\,\mu$s with $T_S = 7\,\mu$s. The blue bars from $t = 0$–$6\,\mu$s show five distinct temporal modes whose height are divided by 200. The green bars show the two-level AFC echo divided by 5, while the red bars show the three-level echo. The echoes show clearly the five distinct temporal modes. Inset: three-level efficiency versus mode number. For one mode $\tau = 3\,\mu$s and for each increase in temporal mode number an additional μs is programmed for the AFC storage time.

higher efficiencies can be achieved. Despite the low efficiency observed, this is to the best of our knowledge the first reported demonstration of spin-wave storage of more than two temporal modes in a doped crystal.

4. Discussion

Although spin-wave storage with an echo efficiency of $\eta_{3LE} = 5.6\%$ is, to our knowledge, the highest efficiency reported so far, a significant increase in this efficiency is required to be viable for quantum communication. To this end, we have strategies for further efficiency improvement. An increase in optical depth leads to an increase in efficiency. This can be obtained by increasing the physical length of the crystal. Experimentally, preparing a memory with an optically and physically thick crystal is feasible, as demonstrated in [20]. An alternative method for increasing the optical depth is to increase the doping concentration at the risk of a reduced coherence time due to ion–ion interactions.

The efficiency of the AFC scheme is limited to 54% in the forward direction due to reabsorption of the emitted light. However, in principle, the efficiency can be increased to unity by retrieving the echo in the backward direction [38]. It is realized by the use of counter-propagating control pulses, which for the present setup is readily achievable.

In this paper, the coherent transfer was mediated by the use of fixed-frequency, temporally square transfer π-pulses. The transfer efficiency is given by the available Rabi frequency, which is limited by the available laser intensity. Thus, one option to increase the Rabi frequency is to directly increase the control intensity by increasing the laser power or by using smaller beams. However, as described in [40], the transfer efficiency can be optimized with the use of control pulses with a hyperbolic tangent frequency chirp and a hyperbolic secant temporal shape. The benefit is that chirped pulses require less intensity than fixed-frequency π-pulses, for a given transfer efficiency.

An alternative method for increasing the efficiency is to place the crystal in an 'impedance matched' cavity, as proposed in [59, 60] and recently demonstrated in [61]. In principle, the input light can be completely absorbed with a readout efficiency limited only by atomic dephasing.

Our memory time was limited to around 20 μs due to the inhomogeneous spin broadening. The storage time can be improved by the use of RF spin echo techniques. Such techniques counteract the effect of dephasing that is introduced by the inhomogeneity of the spin state. Dynamical decoupling techniques have been implemented successfully in $Pr^{3+} : Y_2SiO_5$ [46, 47], $Pr^{3+} : La_2(WO_4)_3$ [62] and $Tm^{3+} : YAG$ [63]. A further increase in storage time can result from the elimination of decoherence sources. For solid state systems, the coherence time can be increased by the application of an external magnetic field of a specific magnitude and angle [44, 64]. In doing so, the first-order Zeeman shift becomes vanishingly small, reducing the sensitivity of the Pr^{3+} ions to the host spins. However, this lifts the degeneracy of the hyperfine levels, which could reduce the available bandwidth for the memory.

We note that, for our experiment, the excited state efficiency η_{AFC} for longer storage times and hence the multimode capacity will benefit from a narrower band laser. Our laser was limited to producing AFC echoes efficiently ($\sim$1%) for storage times of up to 7 μs.

The next experimental milestone regarding this memory is the storage of single-photon level light and non-classical light into a single spin-wave excitation. The results reported here were obtained with the use of bright input pulses, but, in principle, can be extended to the quantum light regime as AFC echo memories scale linearly with input power and are, in principle, noise-free [19]. As well as increasing the efficiency, the major experimental challenge is to filter out pollutive light from the echo mode emitted from other hyperfine levels. This is particularly difficult in $Pr^{3+} : Y_2SiO_5$ as the hyperfine levels occur only 10 MHz away from the signal frequency. For this, narrow band filtering would be required, for which a $Pr^{3+} : Y_2SiO_5$ crystal is ideally suited, as demonstrated in [35, 65].

5. Conclusions

In conclusion, we have reported on coherent and multi-temporal mode storage of light using the full AFC memory scheme. Using this scheme, a total efficiency of $\eta_{3\mathrm{LE}} = 5.6\%$ was observed, the highest efficiency reported so far. The coherent nature of the spin-wave storage is shown for the first time using a time-bin interference measurement resulting in an average visibility of 81.7%, independent of the storage time. A total of five temporal modes was stored and recalled on-demand from the memory, the highest number of modes stored as a spin wave in a doped crystal. We discussed ways to improve the efficiency and storage time further and the extendibility to the single-photon regime.

Acknowledgments

Financial support from the European projects CHIST-ERA QScale and FP7-CIPRIS (MC ITN-287252), as well as from the ERC starting grant QuLIMA, is acknowledged. MM acknowledges the Beatriu de Pinós program (2010BP B0014) for financial support.

References

[1] Briegel H-J, Dür W, Cirac J I and Zoller P 1998 Quantum repeaters: the role of imperfect local operations in quantum communication *Phys. Rev. Lett.* **81** 5932–5

[2] Duan L-M, Lukin M D, Cirac J I and Zoller P 2001 Long-distance quantum communication with atomic ensembles and linear optics *Nature* **414** 413–8

[3] Sangouard N, Simon C, de Riedmatten H and Gisin N 2011 Quantum repeaters based on atomic ensembles and linear optics *Rev. Mod. Phys.* **83** 33–80

[4] Kok P, Munro W J, Nemoto K, Ralph T C, Dowling J P and Milburn G J 2007 Linear optical quantum computing with photonic qubits *Rev. Mod. Phys.* **79** 135–74

[5] Matsukevich D N, Chanelière T, Jenkins S D, Lan S-Y, Kennedy T A B and Kuzmich A 2006 Deterministic single photons via conditional quantum evolution *Phys. Rev. Lett.* **97** 013601

[6] Nunn J, Langford N K, Kolthammer W S, Champion T F M, Sprague M R, Michelberger P S, Jin X-M, England D G and Walmsley I A 2013 Enhancing multiphoton rates with quantum memories *Phys. Rev. Lett.* **100** 133601

[7] Specht H P, Nolleke C, Reiserer A, Uphoff M, Figueroa E, Ritter S and Rempe G 2011 A single-atom quantum memory *Nature* **473** 190–3

[8] Simon C *et al* 2010 Quantum memories *Eur. Phys. J.* D **58** 1–22

[9] Chanelière T, Matsukevich D N, Jenkins S D, Lan S-Y, Kennedy T A B and Kuzmich A 2005 Storage and retrieval of single photons transmitted between remote quantum memories *Nature* **438** 833–6

[10] Chou C W, de Riedmatten H, Felinto D, Polyakov S V, van Enk S J and Kimble H J 2005 Measurement-induced entanglement for excitation stored in remote atomic ensembles *Nature* **438** 828–32

[11] Simon J, Tanji H, Thompson J K and Vuletić V 2007 Interfacing collective atomic excitations and single photons *Phys. Rev. Lett.* **98** 183601

[12] Choi K S, Deng H, Laurat J and Kimble H J 2008 Mapping photonic entanglement into and out of a quantum memory *Nature* **452** 67–71

[13] Radnaev A G, Dudin Y O, Zhao R, Jen H H, Jenkins S D, Kuzmich A and Kennedy T A B 2010 A quantum memory with telecom-wavelength conversion *Nature Phys.* **6** 894–9

[14] Bao X-H, Reingrubern A, Dietrich P, Rui J, Dück A, Strassel T, Li L, Liu N-L, Zhao B and Pan J-W 2012 Efficient and long-lived quantum memory with cold atoms inside a ring cavity *Nature Phys.* **8** 517–21

[15] Julsgaard B, Sherson J, Cirac J I, Fiurášek J and Polzik E S 2004 Experimental demonstration of quantum memory for light *Nature* **432** 482–6

[16] Eisaman M D, André A, Massou F, Fleischhauer M, Zibrov A S and Lukin M D 2005 Electromagnetically induced transparency with tunable single-photon pulses *Nature* **438** 837–41

[17] Reim K F, Michelberger P, Lee K C, Nunn J, Langford N K and Walmsley I A 2011 Single-photon-level quantum memory at room temperature *Phys. Rev. Lett.* **107** 053603

[18] Hosseini M, Campbell G, Sparkes B M, Lam P K and Buchler B C 2011 Unconditional room-temperature quantum memory *Nature Phys.* **7** 794–8

[19] de Riedmatten H, Afzelius M, Staudt M U, Simon C and Gisin N 2008 A solid-state light–matter interface at the single-photon level *Nature* **456** 773–7

[20] Hedges M P, Longdell J J, Li Y and Sellars M J 2010 Efficient quantum memory for light *Nature* **465** 1052

[21] Amari A *et al* 2010 Towards an efficient atomic frequency comb quantum memory *J. Lumin.* **130** 1579–85

[22] Sabooni M, Beaudoin F, Walther A, Lin N, Amari A, Huang M and Kröll S 2010 Storage and recall of weak coherent optical pulses with an efficiency of 25% *Phys. Rev. Lett.* **105** 060501

[23] Chanelière T, Ruggiero J, Bonarota M, Afzelius M and Gouët J-L L 2010 Efficient light storage in a crystal using an atomic frequency comb *New J. Phys.* **12** 023025

[24] Lauritzen B, Minář J, de Riedmatten H, Afzelius M, Sangouard N, Simon C and Gisin N 2010 Telecommunication-wavelength solid-state memory at the single photon level *Phys. Rev. Lett.* **104** 080502

[25] Usmani I, Afzelius M, de Riedmatten H and Gisin N 2010 Mapping multiple photonic qubits into and out of one solid-state atomic ensemble *Nature Commun.* **1** 12
[26] Bonarota M, Gouët J-L L and Chanelière T 2011 Highly multimode storage in a crystal *New J. Phys.* **13** 013013
[27] Clausen C, Usmani I, Bussières F, Sangouard N, Afzelius M, de Riedmatten H and Gisin N 2011 Quantum storage of photonic entanglement in a crystal *Nature* **469** 508–11
[28] Saglamyurek E, Sinclair N, Jin J, Slater J A, Oblak D, Bussières F, George M, Ricken R, Sohler W and Tittel W 2011 Broadband waveguide quantum memory for entangled photons *Nature* **469** 512–5
[29] Usmani I, Clausen C, Bussières F, Sangouard N, Afzelius M and Gisin N 2012 Heralded quantum entanglement between two crystals *Nature Photon.* **6** 234
[30] Saglamyurek E, Sinclair N, Jin J, Slater J A, Oblak D, Bussières F, George M, Ricken R, Sohler W and Tittel W 2012 Conditional detection of pure quantum states of light after storage in a Tm-doped waveguide *Phys. Rev. Lett.* **108** 083602
[31] Gündoğan M, Ledingham P M, Almasi A, Cristiani M and de Riedmatten H 2012 Quantum storage of a photonic polarization qubit in a solid *Phys. Rev. Lett.* **108** 190504
[32] Clausen C, Bussières F, Afzelius M and Gisin N 2012 Quantum storage of heralded polarization qubits in birefringent and anisotropically absorbing materials *Phys. Rev. Lett.* **108** 190503
[33] Zhou Z-Q, Lin W-B, Yang M, Li C-F and Guo G-C 2012 Realization of reliable solid-state quantum memory for photonic polarization qubit *Phys. Rev. Lett.* **108** 190505
[34] Ledingham P M, Naylor W R and Longdell J J 2012 Experimental realization of light with time-separated correlations by rephasing amplified spontaneous emission *Phys. Rev. Lett.* **109** 093602
[35] Beavan S E, Hedges M P and Sellars M J 2012 Demonstration of photon-echo rephasing of spontaneous emission *Phys. Rev. Lett.* **109** 093603
[36] McAuslan D L, Ledingham P M, Naylor W R, Beavan S E, Hedges M P, Sellars M J and Longdell J J 2011 Photon-echo quantum memories in inhomogeneously broadened two-level atoms *Phys. Rev.* A **84** 022309
[37] Damon V, Bonarota M, Louchet-Chauvet A, Chanelière T and Gouët J-L L 2011 Revival of silenced echo and quantum memory for light *New J. Phys.* **13** 093031
[38] Afzelius M, Simon C, de Riedmatten H and Gisin N 2009 Multimode quantum memory based on atomic frequency combs *Phys. Rev.* A **79** 052329
[39] Afzelius M, Usmani I, Amari A, Lauritzen B, Walther A, Simon C, Sangouard N, Minář J, de Riedmatten H, Gisin N and Kröll S 2010 Demonstration of atomic frequency comb memory for light with spin-wave storage *Phys. Rev. Lett.* **104** 040503
[40] Minář J, Sangouard N, Afzelius M, de Riedmatten H and Gisin N 2010 Spin-wave storage using chirped control fields in atomic frequency comb-based quantum memory *Phys. Rev.* A **82** 042309
[41] Timoney N, Lauritzen B, Usmani I, Afzelius M and Gisin N 2012 Atomic frequency comb memory with spin-wave storage in $^{153}Eu^{3+} : Y_2SiO_5$ *J. Phys. B: At. Mol. Opt. Phys.* **45** 124001
[42] Equall R W, Cone R L and Macfarlane R M 1995 Homogeneous broadening and hyperfine structure of optical transitions in $Pr^{3+} : Y_2SiO_5$ *Phys. Rev.* B **52** 3963–9
[43] Sun Y 2005 Rare earth materials in optical storage and data processing applications *Spectroscopic Properties of Rare Earths in Optical Materials* ed G Liu and B Jacquier (Berlin: Springer) pp 395–6
[44] Fraval E, Sellars M J and Longdell J J 2004 Method of extending hyperfine coherence times in $Pr^{3+} : Y_2SiO_5$ *Phys. Rev. Lett.* **92** 077601
[45] Souza A M, Álvarez A G and Suter D 2011 Robust dynamical decoupling for quantum computing and quantum memory *Phys. Rev. Lett.* **106** 240501
[46] Longdell J J, Fraval E, Sellars M J and Manson N B 2005 Stopped light with storage times greater than one second using electromagnetically induced transparency in a solid *Phys. Rev. Lett.* **95** 063601
[47] Fraval E, Sellars M J and Longdell J J 2005 Dynamic decoherence control of a solid-state nuclear-quadrupole qubit *Phys. Rev. Lett.* **95** 030506

[48] Drever R W P, Hall J L, Kowalski F V, Hough J, Ford G M, Munley A J and Ward H 1983 Laser phase and frequency stabilization using an optical resonator *Appl. Phys.* B **31** 97
[49] Nilsson M, Rippe L, Kröll S, Klieber R and Suter D 2004 Hole-burning techniques for isolation and study of individual hyperfine transitions in inhomogeneously broadened solids demonstrated in Pr^{3+} : Y_2SiO_5 *Phys. Rev.* B **70** 214116
[50] Guillot-Noël O, Goldner P, Du Y L, Loiseau P, Julsgaard B, Rippe L and Kröll S 2007 Hyperfine structure, optical dephasing and spectral-hole lifetime of single-crystalline Pr^{3+} : $La_2(WO_4)_3$ *Phys. Rev.* B **75** 205110
[51] Ham B S and Hemmer P R 2003 Population shelved all-optical modulation *Phys. Rev.* B **68** 073102
[52] Allen L and Eberly J H 1975 *Optical Resonance and Two-Level Atoms* (New York: Wiley)
[53] Scully M O and Zubairy M S 1997 *Quantum Optics* (Cambridge: Cambridge University Press)
[54] Lauritzen B, Timoney N, Gisin N, Afzelius M, de Riedmatten H, Sun Y, Macfarlane R M and Cone R L 2012 Spectroscopic investigations of Eu^{3+} : Y_2SiO_5 for quantum memory applications *Phys. Rev.* B **85** 115111
[55] Gisin N, Ribordy G, Tittel W and Zbinden H 2002 Quantum cryptography *Rev. Mod. Phys.* **74** 145–95
[56] Staudt M U, Hastings-Simon S R, Nilsson M, Afzelius M, Scarani V, Ricken R, Suche H, Sohler W, Tittel W and Gisin N 2007 Fidelity of an optical memory based on stimulated photon echoes *Phys. Rev. Lett.* **98** 113601
[57] Staudt M U, Afzelius M, de Riedmatten H, Hastings-Simon S R, Simon C, Ricken R, Suche H, Sohler W and Gisin N 2007 Interference of multimode photon echoes generated in spatially separated solid-state atomic ensembles *Phys. Rev. Lett.* **99** 173602
[58] Simon C, de Riedmatten H, Afzelius M, Sangouard N, Zbinden H and Gisin N 2007 Quantum repeaters with photon pair sources and multimode memories *Phys. Rev. Lett.* **98** 190503
[59] Afzelius M and Simon C 2010 Impedance-matched cavity quantum memory *Phys. Rev.* A **82** 022310
[60] Moiseev S A, Andrianov S N and Gubaidullin F F 2010 Efficient multimode quantum memory based on photon echo in an optimal QED cavity *Phys. Rev.* A **82** 022311
[61] Sabooni M, Li Q, Kröll S and Rippe L 2013 Efficient quantum memory using a weakly absorbing sample *Phys. Rev. Lett.* **110** 133604
[62] Lovrić M, Suter D, Ferrier A and Goldner P 2013 Faithful solid state optical memory with dynamically decoupled spin wave storage arXiv:1302.3358
[63] Pascual-Winter M F, Tongning R-C, Chanelière T and Le Gouët J-L 2012 Spin coherence lifetime extension in Tm^{3+} : YAG through dynamical decoupling *Phys. Rev.* B **86** 184301
[64] Heinze G, Mieth S and Halfmann T 2011 Control of dark-state polariton collapses in a doped crystal *Phys. Rev.* A **84** 013827
[65] Zhang H, Sabooni M, Rippe L, Kim C, Kröll S, Wang L V and Hemmer P R 2012 Slow light for deep tissue imaging with ultrasound modulation *Appl. Phys. Lett.* **100** 131102